Predicting buckling resistance of two three-dimensional lattice architectures

Predicting buckling resistance of two three-dimensional lattice architectures

Luca Raimondi[a *], Luca Tomesani[a], Andrea Zucchelli[a]

[a]*DIN – Università di Bologna, Viale Risorgimento 2, 40136 Bologna, Italia*

[+]

Corresponding authors:
Luca Raimondi
E-mail address: luca.raimondi@unibo.it

Abstract

Lattice structures are an important class of architected cellular solids and structures with high potential for multifunctional and lightweight applications. Novel technologies such as additive manufacturing have vastly extended the design freedom to develop such architectures. In this work, a reliable theoretical model for optimizing unit cell design against buckling is developed for two different cell architectures: pyramidal and tetrahedral. The model's accuracy was evaluated through extensive finite element analysis and compared to existing methods available in the literature.

Keywords:

Lattices; Cellular solids; Buckling failure; Topology effects; Finite Element Analysis (FEA)**;**

1. Introduction

Cellular Solids and Structures (CSSs) are a class of metamaterial with increasing interest in several industrial sectors thanks to their unique possibility to extend the constitutive material property space by a tailored design of their mesostructure [1]. Because of their flexibility, engineered CSSs have recently found increasing applications in transport (e.g., aerospace [2]–[6], mobility [7], [8], rail [9], [10]) as well as in the biomedical sector [11].

At their mesoscale, i.e. in a range spanning from 0.1 [mm] to 10 [mm], CSSs materials essentially consist of an interconnected network of struts or plates that form the edges and faces of the unit cell [12]; a CSSs is, in this context, a theoretically infinite periodic cluster of unit cells that are packed together form the solid metamaterial. Architected CSSs are often referred to as lattice structures (LS), mainly comprised of location-specific struts and nodes [13]–[15]. Several new classes of LS were developed by embedding different unit cell architectures at multiple scales: ultra-light/ultra-stiff [16], [17], shape recovering [18], negative Poisson's ratio [19]–[22], close to infinite bulk-to-shear modulus ratios [23], [24], high specific energy absorption [25] or thermal and vibration insulators [26], [27]. Traditional manufacturing methods can be challenging to produce high-complexity cell structures with precise geometries [28]–[31]. The extreme development in additive manufacturing (AM) over the last decades has vastly expanded the design and manufacturing possibilities for creating novel LS [15], [32]–[36] with an ever-increasing level of precision. Due to the specific limitations of each AM process, a deep optimization of the unit cell is required to address printability, support requirements, and material utilization efficiency. Many theoretical, numerical, and experimental bodies were dedicated to designing new lattice arrangements and studying their properties, as documented by several recent studies and reviews [37]–[39]. Ashby, Gibson, Fleck, and Dhespande [40]–[44] are well known for developing closed-form mathematical formulations to describe the performance of LS in terms of Young modulus, yielding stress, and critical buckling load using beam and column theory. Their studies analyzed the unit cell by exploiting symmetry and assuming that the struts were pin-jointed. Although they provide a highly used design framework in selecting unit cell geometric parameters, the accuracy of the results of these analytical models with experimental and numerical results through the finite element method (FEA) is mixed in the literature [35], [45]. Hanks et al. [46] report that analytical models tend to overestimate the modulus compared to FEA.

Moreover, yielding stress predicted by analytical models overlaps with FEA results if bending in struts is negligible. A particularly relevant comment is that the aforementioned analytical models do not account for the contribution of the nodes to the unit cell's overall mechanical properties, as pointed out by Meza and others [47]. Due to the nature of their mesostructure, elastic buckling and plastic yielding are two of the most common failure mechanisms affecting LS's compressive strength. Several studies demonstrate that buckling may occur either at the strut level [48]–[53], at the material level, or in between [54]. Strategies to discriminate at which scale buckling can occur in large CS involve a linear buckling analysis based on Floquet-Bloch wave theory [55], searching over the wave-vector space and analyzing the resulting wavelengths. Herein, a small or large wavelength, compared to the unit cell size, corresponds to microscopic or macroscopic instability, respectively [54]. On the other side, from macroscopic stress-strain curves, changes in slope due to yielding or buckling are challenging to distinguish [53]. Considering that the critical buckling load of a slender column scales by two orders of magnitude with its decreasing radius to yield stress, significant strength improvements can be achieved by optimizing the buckling resistance. Researchers have employed different methods to optimize the unit cell design against critical buckling load P_{cr}. One of the most direct way, as suggested by Deshpande [41] was the adoption of the well known Euler's formula:

$$P_E = \frac{n^2 \pi^3 E_s a^4}{4\, l^2} \tag{1}$$

Being a, l the radius and the length of the strut, E_s the elastic modulus and n a factor depending on the rotational stiffness of the nodes [56]. Despite its apparent simplicity, a proper selection of the coefficient n for Eq. (1) has reported to be challanging (see [53], [57]–[59] amongst others). Moreover, the formula does’n account for the lateral deflections due to the actual prestressed state of the cell under a given loading condition and neglects out-of-plane deformations. Meanwhile, FEA eigenvalue buckling was

adopted by several researchers and found to be consistent with experimental data [37], [60]–[63]. In the attempt to provide a reliable model for optimizing unit cell design against buckling, a closed-form analytical solution that accounts for the general prestressed state of the cell due to the combined effects of bending, shear, torsion, and axial load was derived based on the matrix structural analysis theory, and compared to the existing ones available in the literature. Although FEA and matrix structural analysis theory share similarities, the first one is a numerical technique, while the latter is formulated in closed form. This allows the determination of closed-form analytical solutions for structural problems, enabling a practical framework for the geometrical optimization of beam-based lattice cells. The investigation focuses on two beam-based cell types in this work, specifically the pyramidal and the tetrahedral (see Figure 1). Effects of strut length l, inclination angle ω, and strut diameter d over mechanical propertis are analized in detail.

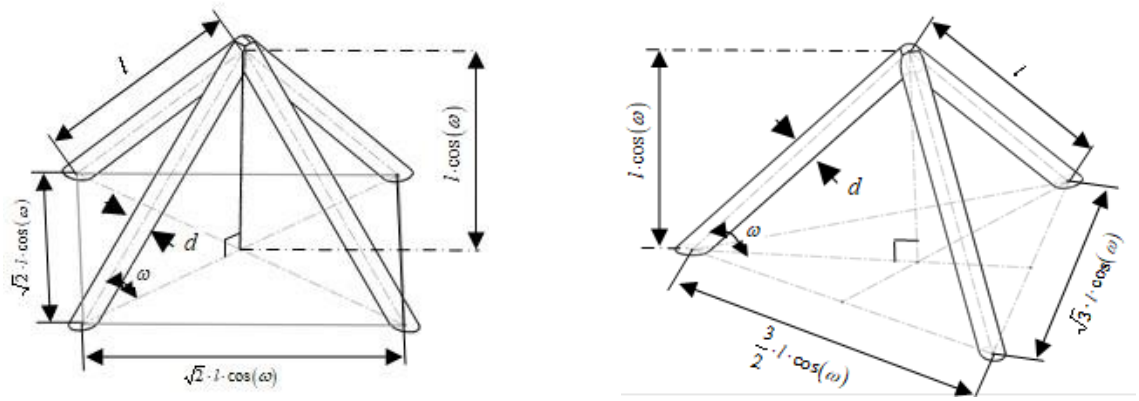

Figure 1: The two-unit cells analyzed in this study with their characteristic dimensions. a) regular pyramidal cell. b) regular tetrahedral cell.

The model's accuracy is benchmarked using FEA analysis, and the effect of the contribution of nodes (pin-jointed or fixed) to mechanical properties is addressed.

2. Materials and Methods

The section is split into three parts. Section 2.1 illustrates the analytical framework used to derive a lattice cell's stiffness, deflection, and internal reaction forces. Next, an analytical model to account for the effects of membrane stress on lateral deflection is

illustrated in section 2.2. Finally, numerical validation methods are illustrated in section 2.3.

2.1. Modeling for prestress analysis

In this work, struts are modeled as interconnected beams with rigid nodes, as shown in Figure 2. To study the influence of shear and rotational bending effects during the deformation of the structure, a 3D Timoshenko beam model was adopted for the analysis.

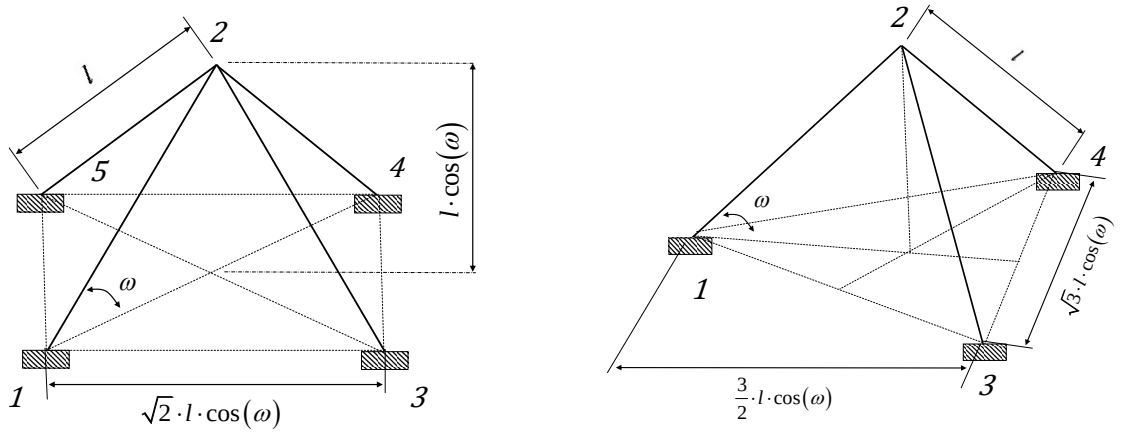

(a) (b)

Figure 2: Beam model of (a) pyramidal and (b) tetrahedral cell with rigid end nodes and built-in constraints

Each node possesses six degrees of freedom, i.e. normal displacement (u_{ix}) two out of axis mutually orthogonal displacements (u_{iy} and u_{iz}), torsion angle (θ_{ix}), and two out of axis mutually orthogonal angles (θ_{iy} and θ_{iz}) (see Figure 3).

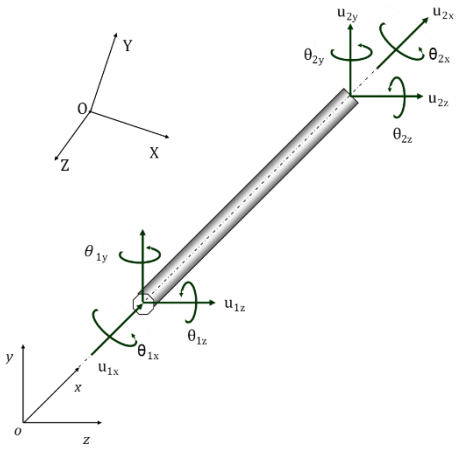

Figure 3: The global ($OXYZ$) and local ($oxyz$) reference system for the 3D beam and local displacement

Respective forces are axial load, two out of axes mutually orthogonal shear load, torque, and two out of axes mutually orthogonal bending moment. In the element reference system, the relationship between generalized forces f and generalized displacement δ at node i and j are:

$$\begin{Bmatrix} f^e{}_i \\ f^e{}_j \end{Bmatrix} = [K]^e \begin{Bmatrix} \delta^e{}_i \\ \delta^e{}_j \end{Bmatrix} \tag{2}$$

A closed-form version of the element stiffness matrix is given in [64] and reported in Eq. A1 of Appendix 1. In Eq. A1, we have denoted with E the Young modulus and with G the shear modulus of the material. A is the cross sectional area, I_y and I_z are the moment of inertia of the cross-section to y and z axis, while I_p is the polar moment of inertia. For cylindrical beams, $A = \frac{\pi d^2}{4}$, $I_y = I_z = \frac{\pi d^4}{64}$ and $I_p = \frac{\pi d^4}{32}$. In Eq. A1, shear stiffness is accounted by $\Phi y = \frac{12\,E\,I_z}{k_s G\,A\,l^2}$ and $\Phi z = \frac{12\,E\,I_y}{k_s G\,A\,l^2}$, where the term k_s is the so-called geometrical factor. For a circular cross-section $k_s = 9/10$ and $\Phi y = \Phi z = \Phi$

Since $[K]^e$ is defined in the local $oxyz$ reference system, while the struct of cells and global displacement are defined in the global $OXYZ$ reference system, a transformation of the stiffness matrix is required. We introduce

$$[\Gamma] = \begin{bmatrix} l_{ox} & m_{ox} & n_{ox} \\ l_{oy} & m_{oy} & n_{oy} \\ l_{oz} & m_{oz} & n_{oz} \end{bmatrix} \tag{3}$$

as the matrix of direction cosines for the ox, oy, oz directions measured in the datum $OXYZ$ reference system. Being $[\Gamma]$ formed by orthonormal unit vectors, $[\Gamma]^T = [\Gamma]^{-1}$. The transformation matrix is thus given by:

$$[T]^e = \begin{bmatrix} [\Gamma] & \mathbf{0} & \mathbf{0} & \mathbf{0} \\ \mathbf{0} & [\Gamma] & \mathbf{0} & \mathbf{0} \\ \mathbf{0} & \mathbf{0} & [\Gamma] & \mathbf{0} \\ \mathbf{0} & \mathbf{0} & \mathbf{0} & [\Gamma] \end{bmatrix} \tag{4}$$

and element stiffness matrix in global coordinates is therefore given by

$$[\bar{K}]^e = [T]^{eT}[K]^e[T]^e \tag{5}$$

The stiffness matrix $[\bar{\mathrm{K}}]$ of the whole structure can be easily obtained by assembling all the element stiffness matrices obtained following the procedure described herein [65]. For both pyramid and tetrahedron, the nodes at the base of the cells were assumed to be built-in constrained. A vertical unit force $F = 1$ [N] was applied at the tip of both cells to retrieve the unknown displacements of the upper node 2 (see Figure 2) by solving the linear system

$$[\bar{K}]\,\{\bar{\Delta}\} = \{\bar{F}\} \tag{6}$$

The displacement vector $\{\bar{\Delta}\}^e$ of each beam in the global reference system was then reconstructed. Nodal forces for each member in the local reference system were calculated using the transformation

$$\{F\} = [K]^e[T]^e\{\bar{\Delta}\}^e \tag{7}$$

Results were stored and used to build the following geometrical stiffness matrix.

2.2. Modelling for buckling

In this work, the effects of membrane stress on lateral deflection are accounted for by a matrix $[Kg]^e$ wich augments the conventional stiffness matrix $[K]^e$. For a beam element, elements of $[Kg]^e$ are generally a function of geometry (such as beam length and shape of the cross-sectional area) and prestressed loading conditions. We call $[Kg]^e$ the geometrical stiffness matrix, although several other definitions are commonly used (such as “stress-stiffness matrix” or “initial stress stiffness matrix”). In literature are reported that different formulations of $[Kg]^e$. In this work, we have adopted the formula reported in Eq. A2 because it accounts for the torsion and is given in a closed-form [66], [67]. The rotation of the geometrical stiffness matrix in the global reference system and assembly procedure is identical to the one explained in the previous Section 2.1. Eigenvalue buckling is based on linear perturbation and can be predicted by using the equation

$$\{P_{cr}\} = 0 + \lambda_i\{\bar{F}\} \tag{8}$$

where $\mathrm{P_{cr}}$ is the critical load at which the straight pre-buckling equilibrium configuration ceases to be a stable state of equilibrium (and an alternate buckling configuration is also

possible at load P_{cr}) and λ_i is the scalar eigenvalue. Eigenvalue buckling formulation is given by

$$[\bar{K}] + \lambda_i[\overline{Kg}]\{\psi_i\} = \{0\} \quad (9)$$

In Eq. (11) $[\bar{K}]$ is the global stiffness matrix, $[\overline{Kg}]$ is the global stress-stiffening matrix, λ_i is the i-th eigenvalue (or load multiplier) and $\{\psi_i\}$ the i-th eigenvector of displacement.

Equations from both Section 2.1 and Section 2.2 were analytically evaluated using the symbolic toolbox of Matlab R2021a to mitigate calculation errors.

2.3. Numerical simulations

Numerical simulations were performed using ANSYS APDL eigenvalue buckling solver to validate the theoretical results by sweeping representative geometrical parameters of both cells. Each beam was meshed using 20 BEAM188 elements. The formulation of the BEAM188 element is based on Timoshenko's beam theory, which includes shear-deformation effects. The element provides options for restrained warping of cross-sections and is suitable for analyzing slender to moderately stubby/thick beam structures. Material was supposed to be a steel, with a young modulus of 200 [GPa] and a poisson ratio $\nu = 0.3$. To validate results from section 2.1, cells with 10 different diameters (0.15 [mm], 0.25 [mm], 0.5 [mm], 0.75 [mm], 1 [mm], 1.25 [mm], 1.5 [mm], 1.75 [mm], 2 [mm], 2.25 [mm] and 2.50 [mm]) and 20 different strut lengths (from 0.5 [mm] to 10 [mm] at incremental steps of 0.5 [mm]) were investigated over varing inclination angle (from 5° to 90° at incremental steps of 2.5°) for a total of 7700 data point per each cell topology. To validate results from section 2.2 cells with 9 different diameters (0.5 [mm], 0.75 [mm], 1 [mm], 1.25 [mm], 1.5 [mm], 1.75 [mm], 2 [mm], 2.25 [mm], 2.50 [mm]) and 20 different strut lengths (from 10 [mm] to 20 [mm] at incremental steps of 1 [mm]) were investigated over varing inclination angle (from 5° to 90° at incremental steps of 2.5°) for a total of 6300 data point per each cell topology.

3. Result and discussion

Results of modeling for the prestress analysis are presented and discussed in Section 3.1, while results of modeling for buckling strength are presented and discussed in Section 3.2

3.1. Modelling for prestress analysis

Calculated deflection of the tip of the pyramidal cell under the vertical unit force exhibits only a vertical component and is reported in Eq. (10)

$$\delta_{pyr} = -\frac{l^3(\Phi+1)}{2E\left(cos(2\omega)\left(12I - Al^2(\Phi+1)\right) + Al^2(\Phi+1) + 12I\right)} \tag{10}$$

and deflection of the tip of the tetrahedral cell under the same loading condition is reported in Eq. (11)

$$\delta_{tet} = -\frac{2l^3(\Phi+1)}{3E\left(cos(2\omega)\left(12I - Al^2(\Phi+1)\right) + Al^2(\Phi+1) + 12I\right)} \tag{11}$$

For the pin-jointed version of both cells, deflection is given by Eq. (12):

$$\delta = -\frac{l}{nEA\ sin^2(\omega)} \tag{12}$$

with $n = 4$ for the pyramidal cell and $n = 3$ for the tetrahedral cell. It is worth mentioning that deflections predicted by both Eq. (10) and Eq. (11) are influenced by the nodal connectivity ("nodal effect"), as demonstrated by the presence of both the moment of inertia I and the quantity Φ. For degenerate cells in which $\omega = {}^{\pi}/_{2}$, from Eq. (10) and Eq. (11) we get $\delta_{pyr} = \frac{l}{4EA}$ and $\delta_{tet} = \frac{l}{3EA}$. This results are consistant with both Eq. (12) and elementary beam theory; due to symmetry the unit force is equally distributed in the 4 rods of the degenerated pyramidal cell and in the 3 rods of the tetrahedral cell. For $\omega = 0$, Eq. (12) returns an infinite, while Eq. (10) and Eq. (11) returns $\delta_{pyr} = -\frac{l^3(\Phi+1)}{48EJ}$ and $\delta_{tet} = -\frac{l^3(\Phi+1)}{36EJ}$ respectively. Neglecting Φ, these deflection are respectively 4 times and 3 times less to the case of a fixed-guided beam subject to a unitary prescribed force [68], thus confirming the validity of the present formulation also in this case. A comparison of the 7700 FEA results for the deflection of the pyramidal cell and correspondent results

obtained by Eq. (10) and Eq. (12) is presented in Figure 4. FEA and Eq. (10) results are in perfect accordance with all the investigated combinations of l, ω and d. Minor discrepancies between FEA and Eq. (10) results are visible for the highest values of l combined with minimal values of ω. Results from FEA, Eq. (10), and Eq. (12) overlap only for the smallest diameter used in the investigation, i.e. $d = 0.15$ [mm]. Meanwhile, it can be observed that FEA and Eq. (12) general trends tend to diverge as the diameter increases. It can be argued that for negligible bending and shear stiffness Eq. (12) is appropriate to describe the stiffness of the pyramidal cell, especially for relatively large inclination angles ω and relatively small struts length l. A comparison of the 7700 FEA results for the deflection of the tetrahedral cell and correspondent results obtained by Eq. (11) and Eq. (12) is presented in Figure 5.

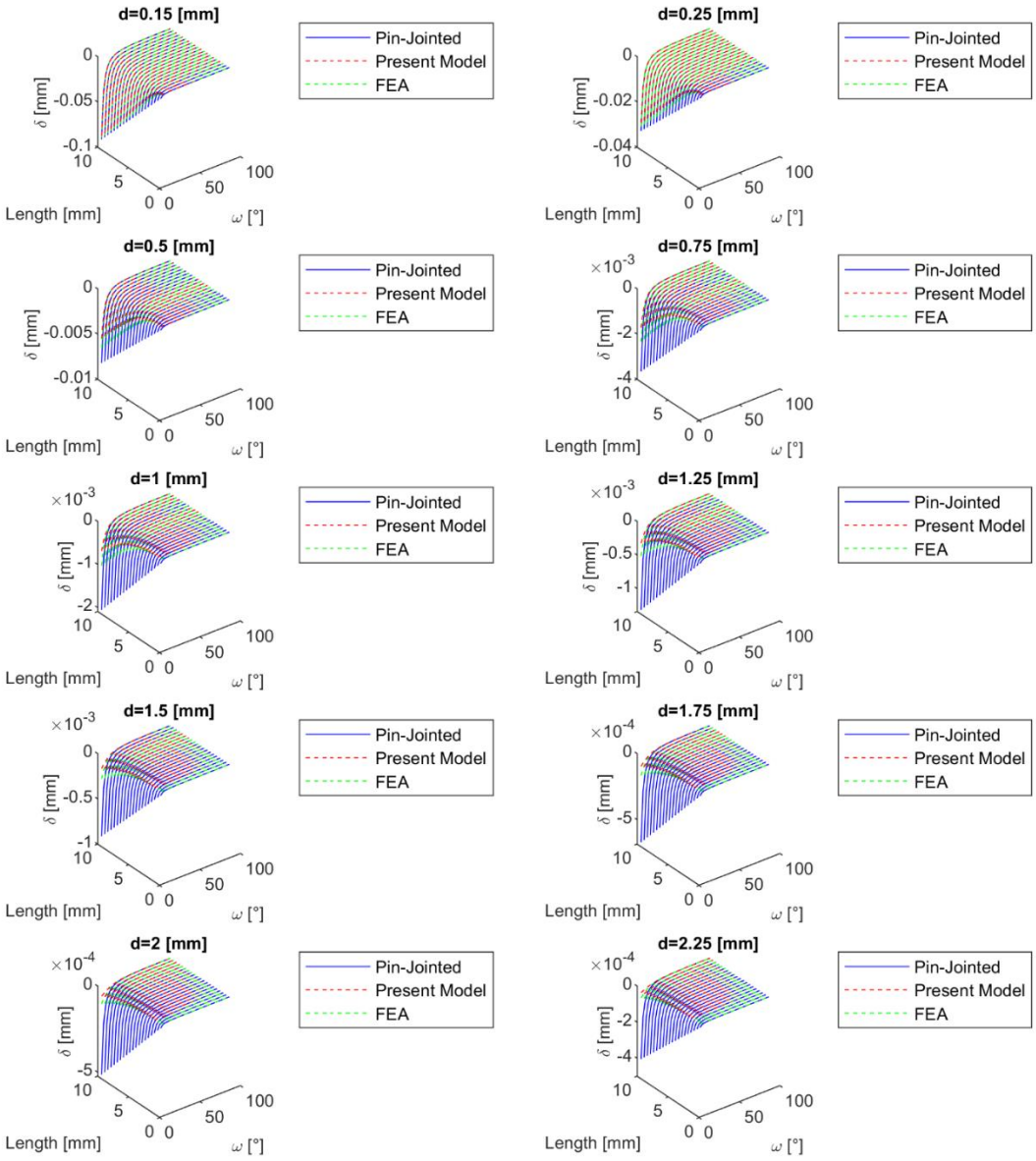

Figure 4: Deflection of the pyramidal cell. Comparison between FEA model, Pin-Jointed model, and present model

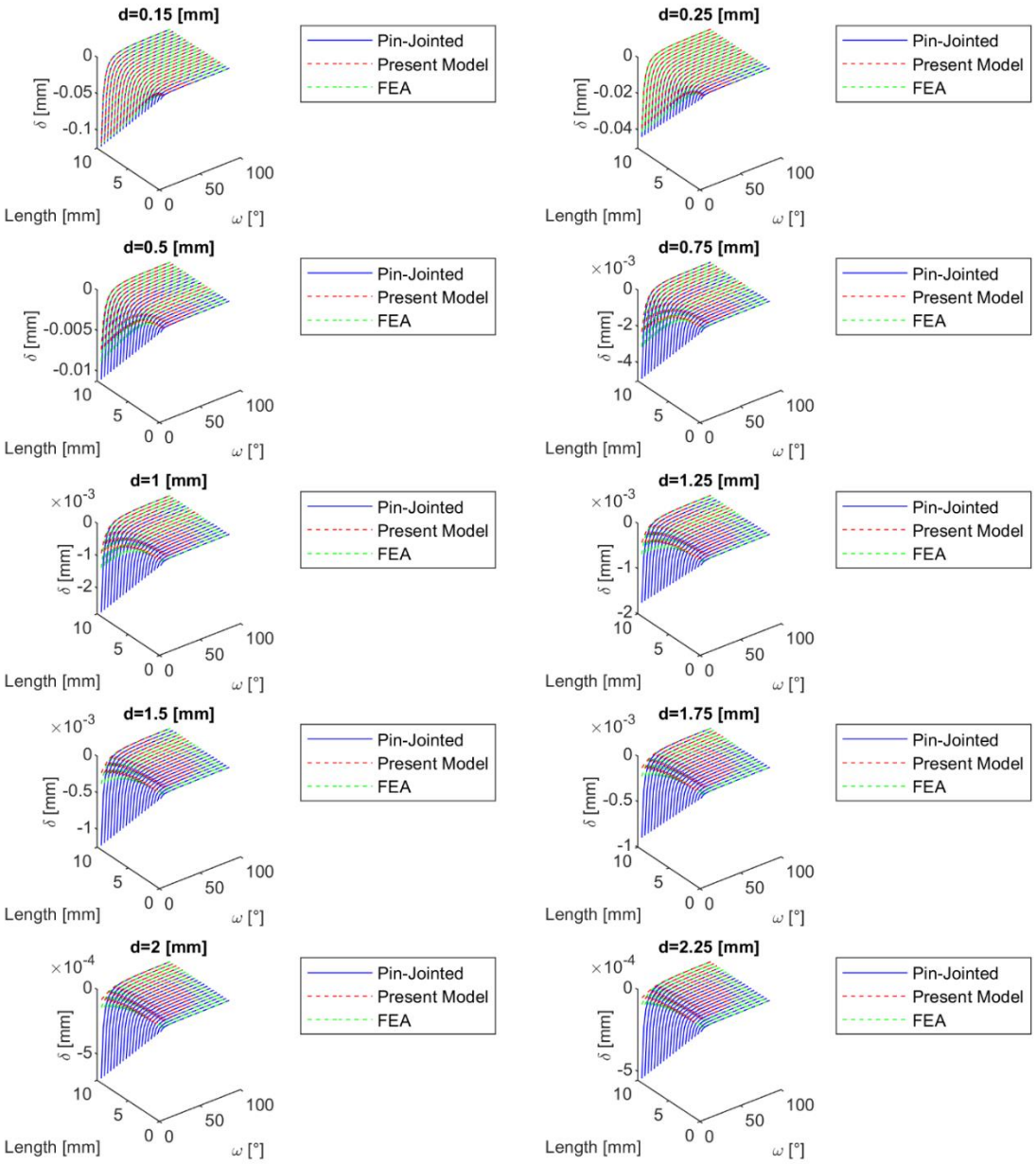

Figure 5: Deflection of the tetrahedral cell. Comparison between FEA model, Pin-Jointed model, and present model

The deflection predicted by all models is higher in the tetrahedral cell compared to the deflection of the pyramidal one. Again, results from FEA, Eq. (11), and Eq. (12) overlap only for the smallest diameter used in the investigation, i.e. $d = 0.15$ [mm]. As observed above, for small inclination angles, formulations including bending and shear, such as FEA and Eq. (11), predicts more reduced deflections than the one provided by Eq. (12). Again, the deviation between FEA and the simplified calculation framework obtained by studying the pin-jointed version of the cell increases with increasing strut length and diameter. It is worth mentioning that according to the Maxwell stability criterion, both cells are conventional classified to be "stretch dominated". From the results retrieved in this section, this conventional definition is ambiguous. Results strengthen the words of Meza and others [47] when they state that "the existing classification of lattice topologies as stretching- or bending-dominated is insufficient and new theories must be developed". Nodal forces in the element reference system for the pyramidal cell are given in Eq. (13)

$$\begin{Bmatrix} F_{1x} \\ F_{1y} \\ F_{1z} \\ M_{1x} \\ M_{1y} \\ M_{1z} \\ F_{2x} \\ F_{2y} \\ F_{2z} \\ M_{2x} \\ M_{2y} \\ M_{2z} \end{Bmatrix} = \begin{Bmatrix} \frac{2Al^2(\Phi+1)\sin(\omega)}{3\left(\cos(2\omega)\left(12I - Al^2(\Phi+1)\right) + Al^2(\Phi+1) + 12I\right)} \\ -\frac{8Il\sqrt{\cos^2(\omega)}}{\sqrt{l^2}\left(\cos(2\omega)\left(Al^2(\Phi+1) - 12I\right) - Al^2(\Phi+1) - 12I\right)} \\ 0 \\ 0 \\ 0 \\ \frac{4Il\sqrt{\cos^2(\omega)}}{\cos(2\omega)\left(12I - Al^2(\Phi+1)\right) + Al^2(\Phi+1) + 12I} \\ -\frac{2Al^2(\Phi+1)\sin(\omega)}{3\left(\cos(2\omega)\left(12I - Al^2(\Phi+1)\right) + Al^2(\Phi+1) + 12I\right)} \\ \frac{8Il\sqrt{\cos^2(\omega)}}{\sqrt{l^2}\left(\cos(2\omega)\left(Al^2(\Phi+1) - 12I\right) - Al^2(\Phi+1) - 12I\right)} \\ 0 \\ 0 \\ 0 \\ \frac{4Il\sqrt{\cos^2(\omega)}}{\cos(2\omega)\left(12I - Al^2(\Phi+1)\right) + Al^2(\Phi+1) + 12I} \end{Bmatrix} \quad (13)$$

For the investigated loading condition, all struts exhibit the same nodal reaction in their respective element system for the pyramidal cell due to symmetry. Nodal forces in the element reference system for the tetrahedral cell are reported in Eq (14)

$$\begin{Bmatrix} F_{1x} \\ F_{1y} \\ F_{1z} \\ M_{1x} \\ M_{1y} \\ M_{1z} \\ F_{2x} \\ F_{2y} \\ F_{2z} \\ M_{2x} \\ M_{2y} \\ M_{2z} \end{Bmatrix} == \begin{Bmatrix} \frac{Al^2(\Phi+1)\sin(\omega)}{2\left(\cos(2\omega)\left(12I - Al^2(\Phi+1)\right) + Al^2(\Phi+1) + 12I\right)} \\ -\frac{6Il\sqrt{\cos^2(\omega)}}{\sqrt{l^2}(\cos(2\omega)\,(Al^2(\Phi+1) - 12I) - Al^2(\Phi+1) - 12I)} \\ 0 \\ 0 \\ 0 \\ \frac{3Il\sqrt{\cos^2(\omega)}}{\cos(2\omega)\left(12I - Al^2(\Phi+1)\right) + Al^2(\Phi+1) + 12I} \\ -\frac{Al^2(\Phi+1)\sin(\omega)}{2\left(\cos(2\omega)\left(12I - Al^2(\Phi+1)\right) + Al^2(\Phi+1) + 12I\right)} \\ \frac{6Il\sqrt{\cos^2(\omega)}}{\sqrt{l^2}(\cos(2\omega)\,(Al^2(\Phi+1) - 12I) - Al^2(\Phi+1) - 12I)} \\ 0 \\ 0 \\ 0 \\ \frac{3Il\sqrt{\cos^2(\omega)}}{\cos(2\omega)\left(12I - Al^2(\Phi+1)\right) + Al^2(\Phi+1) + 12I} \end{Bmatrix} \quad (14)$$

Also in this case, all struts exhibit the same nodal reaction in their respective element system for the pyramidal cell due to symmetry.

3.2. Modeling for buckling

Eigenvalue buckling analysis had a high computational cost, and some simplifications in the formulas were requested. The area A was the only maintained unknown parameter related to the cross-section ($I_y = I_z = \frac{A^2}{4\,\pi}$ and $I_p = \frac{A^2}{2\,\pi}$). Under these assumptions, the 4 independent critical loads predicted by the present model for the pyramidal cell are:

$$\begin{aligned} P_{cr1} = {} & (15A^2\csc(\omega)(6A(6AE(\mathrm{E}^2 - \mathrm{E}G + 2G^2) + G\csc^2(\omega)(12A\mathrm{E}^2 + \pi G\mathrm{l}^2(16\mathrm{E} - 4G\omega\cos \\ & + G)) + 2\mathrm{E}\cos(2\omega)(3A(\mathrm{E} - 2G)(\mathrm{E} - G) + \pi G\mathrm{l}^2(5\mathrm{E} - 8G)) + 2\pi\mathrm{E}G\mathrm{l}^2(5\mathrm{E} \\ & - 8G)) + 8\pi^2G^2\mathrm{l}^4((2\mathrm{E} - G)\cos(2\omega) + 2\mathrm{E} + G))/(4(3A\mathrm{E} + \pi G\mathrm{l}^2)(45A^2\mathrm{E} \\ & + \pi\mathrm{l}^2\csc^2(\omega)(3A(4\mathrm{E} + 5G) + 4\pi G\mathrm{l}^2) - 12\pi A\mathrm{E}\mathrm{l}^2 - 4\pi^2G\mathrm{l}^4)) \end{aligned} \quad (15)$$

$$\begin{aligned} P_{cr2} = {} & -((10A(-G\pi l^2 + (G\pi l^2 + 3A(E - G))\cos^2(\omega) - 3AE)(-4EG^2\pi^3\cos^2(\omega)(\cos(2\omega) \\ & - 3)\sin(\omega)l^6 - 6AG\pi^2\sin(\omega)((2E - G)((4E - G)\cos^4(\omega) + 4(2E \\ & - 3G)\sin^2(\omega)) - 4(4E^2 + 5GE + 3G^2))l^4 - 9A^2E\pi((8E^2 - 23GE \\ & + 4G^2)\cos^4(\omega) - 8E^2 - 54G^2 - 89EG + (-8E^2 + 39GE \\ & - 54G^2)\cos(2\omega))\sin(\omega)l^2 + 27A^3E^2((11E - 12G)\cos^4(\omega) + 17E \\ & + 22G + (22G - 7E)\cos(2\omega))\sin(\omega) + \sqrt{CC}\,))/\,((G\pi l^2 + 3AE)(2(G\pi l^2 \\ & + 3AE)(-4G\pi^2l^4 - 12AE\pi l^2 + 45A^2E)\cos^6(\omega) - 9(-12G^2\pi^3l^6 \\ & + 4AG(5G - 18E)\pi^2l^4 + A^2(-108E^2 + 190GE + 75G^2)\pi l^2 \\ & + 390A^3E^2)\cos^4(\omega) + 20(G\pi l^2 + 3AE)(-14G\pi^2l^4 + 3A(3G - 14E)\pi l^2 \\ & + 54A^2E)\cos^2(\omega) + 180\pi(G\pi l^3 + 3AEl)^2))) \end{aligned} \quad (16)$$

with

$$
\begin{aligned}
CC = {} & (-(-8EG^2\pi^3 l^6 + 6AG(G-2E)(4E+G)\pi^2 l^4 + 9A^2E(-8E^2+13GE+4G^2)\pi l^2 \\
& + 27A^3E^2(9E-8G))^2\cos^{10}(\omega) + (320E^2G^4\pi^6 l^{12} + 384AEG^3(10E^2 \\
& + 3GE - 3G^2)\pi^5 l^{10} + 36A^2G^2(480E^4 + 224GE^3 - 428G^2E^2 + 148G^3E \\
& + 25G^4)\pi^4 l^8 + 108A^3EG(320E^4 + 96GE^3 - 762G^2E^2 + 127G^3E \\
& + 190G^4)\pi^3 l^6 + 81A^4E(320E^5 - 384GE^4 - 2667G^2E^3 + 192G^3E^2 \\
& + 1920G^4E - 600G^5)\pi^2 l^4 - 486A^5E^2(128E^4 + 559GE^3 - 214G^2E^2 \\
& - 530G^3E + 300G^4)\pi l^2 - 13851A^6E^5(9E-8G))\cos^8(\omega) \\
& - 8(64E^2G^4\pi^6 l^{12} + 96AEG^3(8E^2+11GE-4G^2)\pi^5 l^{10} + 36A^2G^2(96E^4 \\
& + 282GE^3 - 72G^2E^2 + 4G^3E + 21G^4)\pi^4 l^8 + 27A^3EG(256E^4 \\
& + 1272GE^3 - 582G^2E^2 - 1201G^3E + 546G^4)\pi^3 l^6 + 81A^4E(64E^5 \\
& + 568GE^4 - 873G^2E^3 - 1879G^3E^2 + 1334G^4E - 150G^5)\pi^2 l^4 \\
& + 243A^5E^2(72E^4 - 512GE^3 - 591G^2E^2 + 766G^3E - 150G^4)\pi l^2 \\
& - 729A^6E^4(61E^2 - 71GE + 6G^2))\cos^6(\omega) + 4(64E^2G^4\pi^6 l^{12} \\
& + 24AEG^3(32E^2 + 150GE - 21G^2)\pi^5 l^{10} + 36A^2G^2(96E^4 + 985GE^3 \\
& + 508G^2E^2 - 160G^3E + 36G^4)\pi^4 l^8 + 108A^3EG(64E^4 + 1155GE^3 \\
& + 1102G^2E^2 - 1740G^3E + 264G^4)\pi^3 l^6 + 81A^4E^2(64E^4 + 2220GE^3 \\
& + 2157G^2E^2 - 9780G^3E + 2784G^4)\pi^2 l^4 + 486A^5E^3(170E^3 + 29GE^2 \\
& - 1720G^2E + 738G^3)\pi l^2 + 729A^6E^4(109E^2 + 20GE + 4G^2))\cos^4(\omega) \\
& - 96AE(G\pi l^2 + 3AE)(76EG^3\pi^4 l^8 + 3AG^2(173E^2 + 524GE - 66G^2)\pi^3 l^6 \\
& + 9A^2EG(118E^2 + 637GE - 528G^2)\pi^2 l^4 + 27A^3E^2(21E^2 + 152GE \\
& - 268G^2)\pi l^2 + 243A^4E^3(13E-2G))\cos^2(\omega) \\
& + 576A^2E^2(G\pi l^2 + 3AE)^2(124G^2\pi^2 l^4 + 99AEG\pi l^2 + 81A^2E^2))
\end{aligned}
\tag{17}
$$

$$
\begin{aligned}
P_{cr3} = {} & -((10A(-G\pi l^2 + (G\pi l^2 + 3A(E-G))\cos^2(\omega) - 3AE)(-4EG^2\pi^3\cos^2(\omega)(\cos(2\omega) \\
& - 3)\sin(\omega) l^6 - 6AG\pi^2\sin(\omega)((2E-G)((4E-G)\cos^4(\omega) + 4(2E \\
& - 3G)\sin^2(\omega)) - 4(4E^2 + 5GE + 3G^2))l^4 - 9A^2E\pi((8E^2 - 23GE \\
& + 4G^2)\cos^4(\omega) - 8E^2 - 54G^2 - 89EG + (-8E^2 + 39GE \\
& - 54G^2)\cos(2\omega))\sin(\omega) l^2 + 27A^3E^2((11E-12G)\cos^4(\omega) + 17E \\
& + 22G + (22G-7E)\cos(2\omega))\sin(\omega) - \sqrt{CC}\,))/((G\pi l^2 + 3AE)(2(G\pi l^2 \\
& + 3AE)(-4G\pi^2 l^4 - 12AE\pi l^2 + 45A^2E)\cos^6(\omega) - 9(-12G^2\pi^3 l^6 \\
& + 4AG(5G-18E)\pi^2 l^4 + A^2(-108E^2 + 190GE + 75G^2)\pi l^2 \\
& + 390A^3E^2)\cos^4(\omega) + 20(G\pi l^2 + 3AE)(-14G\pi^2 l^4 + 3A(3G-14E)\pi l^2 \\
& + 54A^2E)\cos^2(\omega) + 180\pi(G\pi l^3 + 3AEl)^2)))
\end{aligned}
\tag{18}
$$

and

$$
P_{cr4} = \frac{20AE\sin(\omega)(3A(E-G) + 3AG\csc^2(\omega) + \pi G l^2)^2}{(6\csc^2(\omega) - 1)(3AE + \pi G l^2)^2} \tag{19}
$$

Due to the formulas' complexity, it is very challenging to determine if any of the four will always return a minimum value for any combination of length, diameter, inclination, or material parameters. The minimum buckling load will be determined from time to time by analyzing the values of the four P_{cr}. It is worth mentioning that Eq. (16) and Eq. (18) differ only for the sign of the square root of CC given in Eq. (17). Domain of validity of the present formulation is $\left]0, \frac{\pi}{2}\right[$ since for $\omega = 0$ axial load vanish in Eq. (13). For $\omega = \frac{\pi}{2}$ Eq.(19) degenerates in $P_{cr4} = 4AE$ that is less than the critical buckling load provided by Euler's formula (Eq. (1)). After an extensive analysis, it can be assumed that the model presented herein provides buckling loads generally greater than the one predicted with

FEA. It is a classical convergency problem due to the limitation of having used only one beam element to model the struts [69]. A deeper investigation revealed that convergency is archived by refining the strut using two elements. From the point of view of symbolic computation, this would have resulted in a more significant eigenvalue problem, with more eigenvalues and consequently more critical loads to analyze. After extensive investigations, it was observed that differences between FEA and present model results were essentially constant by varying the inclination angle ω for a given length and diameter. Therefore, the minimum critical load was normalized for fixed l and d by dividing its local value by the maximum value assumed by it in the range of variation $\left]0, \frac{\pi}{2}\right[$. This information is of particular interest for optimizing strut inclination to improve cell buckling characteristics. Normalized results provided by Euler buckling, present formulas, and FEA analysis are reported in Figure 6 for the pyramidal cell. It can be observed that conventional formulations based on pin-jointed assumptions systematically fail to identify the optimum inclination angle to improve pyramidal cell buckling resistance. A good accordance between the results obtained by the problem solution formulated in this work and FEA is noticeable. Minor discrepancies exist for small strut slenderness l/d. It can be observed that results overlap for a slenderness ratio greater than 5. Indeed, in the cases where thick-short strut-like members are used, the Poisson's ratio plays an important role, and the model with beam elements could fail in capturing the actual buckling load.

The critical buckling loads obtained for the tetrahedral cell are

$$P_{cr1} = (45A^2\sin(\omega)(3A(E-G) + 3AG\csc^2(\omega) + \pi Gl^2)(E\csc^2(\omega)(3AE + 4\pi Gl^2) - 3AE(E-2G) + 2\pi Gl^2(G-2E)))/(2(3AE + \pi Gl^2)(45A^2E + \pi l^2\csc^2(\omega)(3A(4E+5G) + 4\pi Gl^2) - 12\pi AEl^2 - 4\pi^2Gl^4)) \quad (20)$$

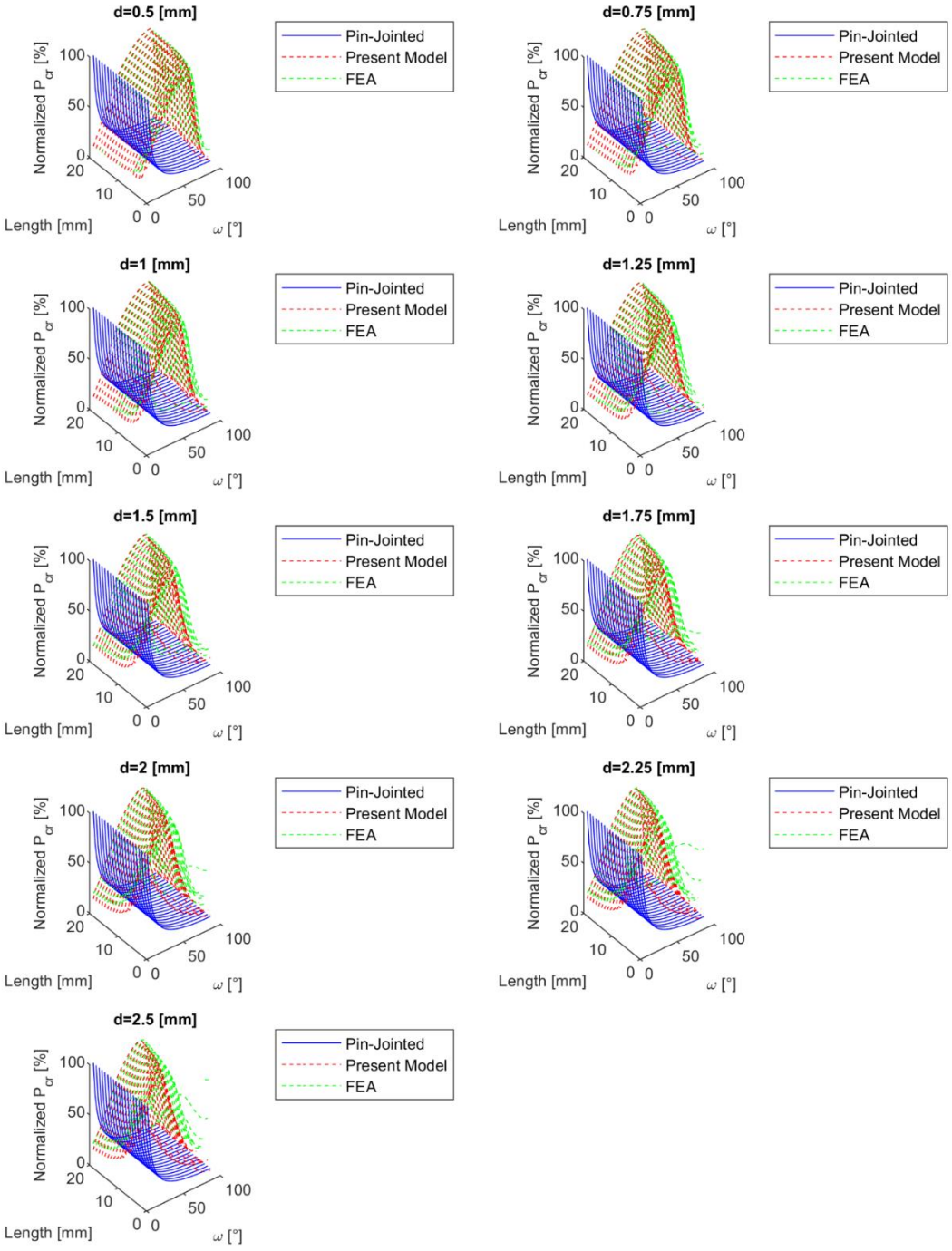

Figure 6: Minimum critical buckling load for the pyramidal cell. Comparison of the results for the pin-jointed model, model presented in this work and FEA results.

$$P_{cr2} = -((15A(-G\pi l^2 + (G\pi l^2 + 3A(E-G))\cos^2(\omega) - 3AE)(-4EG^2\pi^3\cos^2(\omega)(\cos(2\omega) - 3)\sin(\omega)l^6 - 6AG\pi^2((2E - G)\cos^2(\omega)((4E - G)\cos^2(\omega) - 8E + 12G) - 52EG)\sin(\omega)l^4 - 9A^2E\pi((8E^2 - 23GE + 4G^2)\cos^4(\omega) - 2(8E^2 - 39GE + 54G^2)\cos^2(\omega) - 128EG)\sin(\omega)l^2 + 27A^3E^2((11E - 12G)\cos^4(\omega) + (44G - 14E)\cos^2(\omega) + 24E)\sin(\omega) + \sqrt{CC}))/(2(G\pi l^2 + 3AE)(2(G\pi l^2 + 3AE)(-4G\pi^2 l^4 - 12AE\pi l^2 + 45A^2E)\cos^6(\omega) - 9(-12G^2\pi^3 l^6 + 4AG(5G - 18E)\pi^2 l^4 + A^2(-108E^2 + 190GE + 75G^2)\pi l^2 + 390A^3E^2)\cos^4(\omega) + 20(G\pi l^2 + 3AE)(-14G\pi^2 l^4 + 3A(3G - 14E)\pi l^2 + 54A^2E)\cos^2(\omega) + 180\pi(G\pi l^3 + 3AEl)^2))) \quad (21)$$

$$P_{cr3} = -((15A(-G\pi l^2 + (G\pi l^2 + 3A(E-G))\cos^2(\omega) - 3AE)(-4EG^2\pi^3\cos^2(\omega)(\cos(2\omega) - 3)\sin(\omega)l^6 - 6AG\pi^2((2E - G)\cos^2(\omega)((4E - G)\cos^2(\omega) - 8E + 12G) - 52EG)\sin(\omega)l^4 - 9A^2E\pi((8E^2 - 23GE + 4G^2)\cos^4(\omega) - 2(8E^2 - 39GE + 54G^2)\cos^2(\omega) - 128EG)\sin(\omega)l^2 + 27A^3E^2((11E - 12G)\cos^4(\omega) + (44G - 14E)\cos^2(\omega) + 24E)\sin(\omega) - \sqrt{CC}))/(2(G\pi l^2 + 3AE)(2(G\pi l^2 + 3AE)(-4G\pi^2 l^4 - 12AE\pi l^2 + 45A^2E)\cos^6(\omega) - 9(-12G^2\pi^3 l^6 + 4AG(5G - 18E)\pi^2 l^4 + A^2(-108E^2 + 190GE + 75G^2)\pi l^2 + 390A^3E^2)\cos^4(\omega) + 20(G\pi l^2 + 3AE)(-14G\pi^2 l^4 + 3A(3G - 14E)\pi l^2 + 54A^2E)\cos^2(\omega) + 180\pi(G\pi l^3 + 3AEl)^2))) \quad (22)$$

and

$$P_{cr4} = \frac{15AE\sin(\omega)(3A(E-G) + 3AG\csc^2(\omega) + \pi G l^2)^2}{(6\csc^2(\omega) - 1)(3AE + \pi G l^2)^2} \quad (23)$$

Where CC for Eq. (21) and Eq. (22) is identical to the one already seen in the pyramidal cell and given by Eq. (17). Also for the tetrahedral cell, formulas for P_{cr2} and P_{cr3} differs from the square root of CC. Domain of validity is the same provided for the pyramidal cell due to the same considerations. Also in this case, convergency issues were encountered. For the tetrahedral cell, normalized results provided by Euler buckling, present formulas, and FEA analysis are reported in Figure 7. Also in this case, the pin-jointed formulation fails to capture the best inclination angle in any studied configurations. It can be observed that the model is always consistent with FEA results, and, again, the best accuracy is obtained for struts having a slenderness ratio greater than 5.

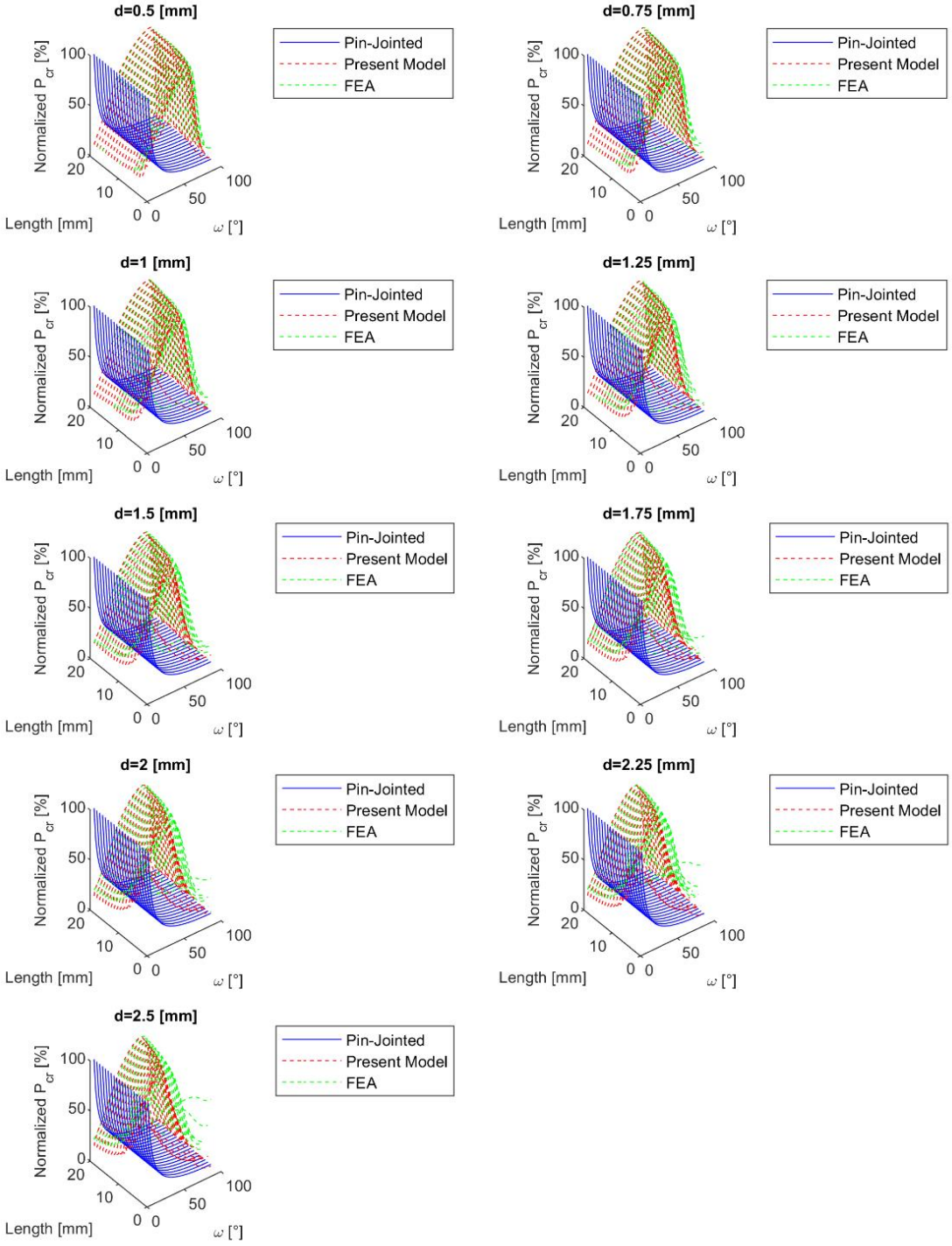

Figure 7: Minimum critical buckling load for the tetrahedral cell. Comparison of the results for the pin-jointed model presented in this work and FEA results.

4. Conclusions

A closed-form analytical framework for optimizing design parameters against the stiffness and buckling of lattice material was developed and applied to two different cell architectures: a pyramidal cell and a tetrahedral cell. Furthermore, closed-form solutions for calculating the compliance and the critical load of both the pyramidal and the tetrahedral cell were obtained and compared to other analytical models available in the literature. FEA results demonstrated the superiority of the models presented in this work in predicting the mechanical properties of the two mentioned cells over conventional analytical models. Furthermore, it was demonstrated that the existing classification of "stretch-dominated" and "bending-dominated" structures is ambiguous and that significant discrepancies between FEA and conventional analytical formulations can be found. Moreover, the analytical model presented in this paper was always consistent with FEA results. In future work, the proposed methodology will be extended to other unit cell types to provide a reliable design framework for optimizing novel LS with improved characteristics.

5. Acknowledgement

The authors kindly acknowledge MIND Srl in Bologna, Italy. Furthermore, a kindly acknowledgement to Graduated Student Dr. Michele Tropeano is given for his help in writing Matlab code.

6. Funding

This work was funded by the H2020 3DP PAN EU project, Project name 3DHYSUS

Declaration of Competing Interest

The authors declare that they have no known competing financial interests or personal relationships that could have appeared to influence the work reported in this paper.

Appendix A1

Both stiffness and geometrical matrix are reported here for the reader's convenience.

$$
[K]^e = \begin{Bmatrix}
\frac{\mathrm{E}\,A}{L} & 0 & 0 & 0 & 0 & 0 & \frac{-\mathrm{E}\,A}{L} & 0 & 0 & 0 & 0 & 0 \\
0 & \frac{12\,\mathrm{E}\,\mathrm{Iz}}{L^3(1+\Phi y)} & 0 & 0 & 0 & \frac{6\,\mathrm{E}\,\mathrm{Iz}}{L^2\,(1+\Phi y)} & 0 & \frac{-12\,\mathrm{E}\,\mathrm{Iz}}{L^3\,(1+\Phi y)} & 0 & 0 & 0 & \frac{6\,\mathrm{E}\,\mathrm{Iz}}{L^2\,(1+\Phi y)} \\
0 & 0 & \frac{12\,\mathrm{E}\,\mathrm{Iy}}{L^3(1+\Phi z)} & 0 & -\frac{6\,\mathrm{E}\,\mathrm{Iy}}{L^2(1+\Phi z)} & 0 & 0 & 0 & \frac{-12\,\mathrm{E}\,\mathrm{Iy}}{L^3\,(1+\Phi z)} & 0 & -\frac{6\,\mathrm{E}\,\mathrm{Iy}}{L^2\,(1+\Phi z)} & 0 \\
0 & 0 & 0 & \frac{G\,\mathrm{Ip}}{L} & 0 & 0 & 0 & 0 & 0 & -\frac{G*\mathrm{Ip}}{L} & 0 & 0 \\
0 & 0 & -\frac{6\,\mathrm{E}\,\mathrm{Iy}}{L^2(1+\Phi z)} & 0 & \frac{(4+\Phi z)\mathrm{E}\,\mathrm{Iy}}{L(1+\Phi z)} & 0 & 0 & 0 & \frac{6\mathrm{E}\,\mathrm{Iy}}{L^2(1+\Phi z)} & 0 & \frac{(2-\Phi z)\mathrm{E}\,\mathrm{Iy}}{L\,(1+\Phi z)} & 0 \\
0 & \frac{6\,\mathrm{E}\,\mathrm{Iz}}{L^2(1+\Phi y)} & 0 & 0 & 0 & \frac{(4+\Phi y)\mathrm{E}\mathrm{Iz}}{L(1+\Phi y)} & 0 & -\frac{6\,\mathrm{E}\,\mathrm{Iz}}{L^2\,(1+\Phi y)} & 0 & 0 & 0 & \frac{(2-\Phi y)\,\mathrm{E}\,\mathrm{Iz}}{L\,(1+\Phi y)} \\
\frac{-\mathrm{E}\,A}{L} & 0 & 0 & 0 & 0 & 0 & \frac{A\,\mathrm{E}}{L} & 0 & 0 & 0 & 0 & 0 \\
0 & -\frac{12\,\mathrm{E}\,\mathrm{Iz}}{L^3(1+\Phi y)} & 0 & 0 & 0 & -\frac{6\,\mathrm{E}\,\mathrm{Iz}}{L^2(1+\Phi y)} & 0 & \frac{12\,\mathrm{E}\,\mathrm{Iz}}{L^3(1+\Phi y)} & 0 & 0 & 0 & -\frac{6\,\mathrm{E}\,\mathrm{Iz}}{L^2(1+\Phi y)} \\
0 & 0 & \frac{-12\mathrm{E}\,\mathrm{Iy}}{L^3(1+\Phi z)} & 0 & \frac{6\mathrm{E}\,\mathrm{Iy}}{L^2(1+\Phi z)} & 0 & 0 & 0 & \frac{12\,\mathrm{E}\,\mathrm{Iy}}{L^3(1+\Phi z)} & 0 & \frac{6\,\mathrm{E}\,\mathrm{Iy}}{L^2\,(1+\Phi z)} & 0 \\
0 & 0 & 0 & -\frac{G*\mathrm{Ip}}{L} & 0 & 0 & 0 & 0 & 0 & \frac{G\,\mathrm{Ip}}{L} & 0 & 0 \\
0 & 0 & -\frac{6\,\mathrm{E}\,\mathrm{Iy}}{L^2(1+\Phi z)} & 0 & \frac{(2-\Phi z)\mathrm{E}\,\mathrm{Iy}}{L\,(1+\Phi z)} & 0 & 0 & 0 & \frac{6\,\mathrm{E}\,\mathrm{Iy}}{L^2(1+\Phi z)} & 0 & \frac{(4+\Phi z)\mathrm{E}\,\mathrm{Iy}}{L(1+\Phi z)} & 0 \\
0 & \frac{6\,\mathrm{E}\,\mathrm{Iz}}{L^2(1+\Phi y)} & 0 & 0 & 0 & \frac{(2-\Phi y)\,\mathrm{E}\,\mathrm{Iz}}{L\,(1+\Phi y)} & 0 & -\frac{6\,\mathrm{E}\,\mathrm{Iz}}{L^2(1+\Phi y)} & 0 & 0 & 0 & \frac{(4+\Phi y)\mathrm{E}\,\mathrm{Iz}}{L(1+\Phi y)}
\end{Bmatrix} \tag{A1}
$$

$$[Kg]^e = \begin{pmatrix}
\frac{F_{x2}}{L} & 0 & 0 & 0 & 0 & 0 & -\frac{F_{x2}}{L} & 0 & 0 & 0 & 0 & 0 \\
0 & \frac{6*F_{x2}}{5*L} & 0 & \frac{M_{y1}}{L} & \frac{M_{x2}}{L} & \frac{F_{x2}}{10} & 0 & -\frac{6*F_{x2}}{5*L} & 0 & \frac{M_{y2}}{L} & -\frac{M_{x2}}{L} & \frac{F_{x2}}{10} \\
0 & 0 & \frac{6*F_{x2}}{5*L} & \frac{M_{z1}}{L} & -\frac{F_{x2}}{10} & \frac{M_{x2}}{L} & 0 & 0 & -\frac{6*F_{x2}}{5*L} & \frac{M_{z2}}{L} & -\frac{F_{x2}}{10} & -\frac{M_{x2}}{L} \\
0 & \frac{M_{y1}}{L} & \frac{M_{z1}}{L} & \frac{F_{x2}*I_p}{A*L} & -\frac{2*M_{z1}-M_{z2}}{6} & \frac{2*M_{y1}-M_{y2}}{6} & 0 & -\frac{M_{y1}}{L} & -\frac{M_{z1}}{L} & -\frac{F_{x2}*I_p}{A*L} & -\frac{M_{z1}+M_{z2}}{6} & \frac{M_{y1}+M_{y2}}{6} \\
0 & \frac{M_{x2}}{L} & -\frac{F_{x2}}{10} & -\frac{2*M_{z1}-M_{z2}}{6} & \frac{2*F_{x2}*L}{15} & 0 & 0 & -\frac{M_{x2}}{L} & \frac{F_{x2}}{10} & -\frac{M_{z1}+M_{z2}}{6} & -\frac{F_{x2}*L}{30} & \frac{M_{x2}}{2} \\
0 & \frac{F_{x2}}{10} & \frac{M_{x2}}{L} & \frac{2*M_{y1}-M_{y2}}{6} & 0 & \frac{2*F_{x2}*L}{15} & 0 & -\frac{F_{x2}}{10} & -\frac{M_{x2}}{L} & \frac{M_{y1}+M_{y2}}{6} & -\frac{M_{x2}}{2} & -\frac{F_{x2}*L}{30} \\
-\frac{F_{x2}}{L} & 0 & 0 & 0 & 0 & 0 & \frac{F_{x2}}{L} & 0 & 0 & 0 & 0 & 0 \\
0 & -\frac{6*F_{x2}}{5*L} & 0 & -\frac{M_{y1}}{L} & -\frac{M_{x2}}{L} & -\frac{F_{x2}}{10} & 0 & \frac{6*F_{x2}}{5*L} & 0 & -\frac{M_{y2}}{L} & \frac{M_{x2}}{L} & -\frac{F_{x2}}{10} \\
0 & 0 & -\frac{6*F_{x2}}{5*L} & -\frac{M_{z1}}{L} & \frac{F_{x2}}{10} & -\frac{M_{x2}}{L} & 0 & 0 & \frac{6*F_{x2}}{5*L} & -\frac{M_{z2}}{L} & \frac{F_{x2}}{10} & \frac{M_{x2}}{L} \\
0 & \frac{M_{y2}}{L} & \frac{M_{z2}}{L} & -\frac{F_{x2}*I_p}{A*L} & -\frac{M_{z1}+M_{z2}}{6} & \frac{M_{y1}+M_{y2}}{6} & 0 & -\frac{M_{y2}}{L} & -\frac{M_{z2}}{L} & \frac{F_{x2}*I_p}{A*L} & \frac{M_{z1}-2*M_{z2}}{6} & -\frac{M_{y1}-2*M_{y2}}{6} \\
0 & -\frac{M_{x2}}{L} & -\frac{F_{x2}}{10} & -\frac{M_{z1}+M_{z2}}{6} & -\frac{F_{x2*L}}{30} & -\frac{M_{x2}}{L} & 0 & \frac{M_{x2}}{L} & \frac{F_{x2}}{10} & \frac{M_{z1}-2*M_{z2}}{6} & \frac{2*F_{x2}*L}{15} & 0 \\
0 & \frac{F_{x2}}{10} & -\frac{M_{x2}}{L} & \frac{M_{y1}+M_{y2}}{6} & \frac{M_{x2}}{L} & -\frac{F_{x2*L}}{30} & 0 & -\frac{F_{x2}}{10} & \frac{M_{x2}}{L} & -\frac{M_{y1}-2*M_{y2}}{6} & 0 & \frac{2*F_{x2*L}}{15}
\end{pmatrix} \quad \text{(A2)}$$

Bibliography

[1] Gibson LJ; Ashby MF, *Cellular solids: structure and properties. 2nd ed.* 1997.

[2] L. Marsavina, “Fracture mechanics of cellular solids,” in *CISM International Centre for Mechanical Sciences, Courses and Lectures*, 2010, pp. 1–46. doi: 10.1007/978-3-7091-0297-8_1.

[3] H. Heo, J. Ju, and D. M. Kim, “Compliant cellular structures: Application to a passive morphing airfoil,” *Compos. Struct.*, vol. 106, pp. 560–569, 2013, doi: 10.1016/j.compstruct.2013.07.013.

[4] K. K. Sairajan, G. S. Aglietti, and K. M. Mani, “A review of multifunctional structure technology for aerospace applications,” *Acta Astronautica*, vol. 120. pp. 30–42, 2016. doi: 10.1016/j.actaastro.2015.11.024.

[5] C. Meola, S. Boccardi, and G. maria Carlomagno, “Composite Materials in the Aeronautical Industry,” in *Infrared Thermography in the Evaluation of Aerospace Composite Materials*, 2017, pp. 1–24. doi: 10.1016/b978-1-78242-171-9.00001-2.

[6] B. Blakey-Milner *et al.*, “Metal additive manufacturing in aerospace: A review,” *Mater. Des.*, vol. 209, 2021, doi: 10.1016/j.matdes.2021.110008.

[7] N. Obaid, M. T. Kortschot, and M. Sain, “Lightweight thermoset foams in automotive applications,” in *Lightweight and Sustainable Materials for Automotive Applications*, 2017, pp. 401–422. doi: 10.1201/9781315152967.

[8] A. Bisht, V. K. Patel, and B. Gangil, “Future of Metal Foam Materials in Automotive Industry,” in *Energy, Environment, and Sustainability*, 2019, pp. 51–63. doi: 10.1007/978-981-15-0434-1_4.

[9] L. Su, H. Liu, G. Yao, and J. Zhang, “Experimental study on the closed-cell

aluminum foam shock absorption layer of a high-speed railway tunnel," *Soil Dyn. Earthq. Eng.*, vol. 119, pp. 331–345, 2019, doi: 10.1016/j.soildyn.2019.01.012.

[10] S. Yao, X. Xiao, P. Xu, Q. Qu, and Q. Che, "The impact performance of honeycomb-filled structures under eccentric loading for subway vehicles," *Thin-Walled Struct.*, vol. 123, pp. 360–370, 2018, doi: 10.1016/j.tws.2017.10.031.

[11] T. Thenard, A. Catapano, R. Allena, M. El May, N. Saintier, and M. Mesnard, "Topography and wettability characterization of surfaces manufactured by SLM and treated by chemical etching," *Mech. Adv. Mater. Struct.*, vol. 29, no. 12, pp. 1674–1691, 2022, doi: 10.1080/15376494.2020.1836292.

[12] L. J. Gibson, "Modelling the mechanical behavior of cellular materials," *Mater. Sci. Eng. A*, vol. 110, no. C, pp. 1–36, 1989, doi: 10.1016/0921-5093(89)90154-8.

[13] M. F. Ashby, "The properties of foams and lattices," *Philos. Trans. R. Soc. A Math. Phys. Eng. Sci.*, vol. 364, no. 1838, pp. 15–30, 2006, doi: 10.1098/rsta.2005.1678.

[14] M. Benedetti, A. du Plessis, R. O. Ritchie, M. Dallago, S. M. J. Razavi, and F. Berto, "Architected cellular materials: A review on their mechanical properties towards fatigue-tolerant design and fabrication," *Mater. Sci. Eng. R Reports*, vol. 144, p. 100606, 2021, doi: 10.1016/j.mser.2021.100606.

[15] T. A. Schaedler and W. B. Carter, "Architected Cellular Materials," *Annual Review of Materials Research*, vol. 46. pp. 187–210, 2016. doi: 10.1146/annurev-matsci-070115-031624.

[16] T. A. Schaedler *et al.*, "Ultralight metallic microlattices," *Science (80-.).*, vol. 334, no. 6058, pp. 962–965, 2011, doi: 10.1126/science.1211649.

[17] S. C. Han, J. W. Lee, and K. Kang, “A New Type of Low Density Material: Shellular,” *Adv. Mater.*, vol. 27, no. 37, pp. 5506–5511, 2015, doi: 10.1002/adma.201501546.

[18] J. T. B. Overvelde *et al.*, “A three-dimensional actuated origami-inspired transformable metamaterial with multiple degrees of freedom,” *Nat. Commun.*, vol. 7, 2016, doi: 10.1038/ncomms10929.

[19] T. Bückmann *et al.*, “Tailored 3D mechanical metamaterials made by dip-in direct-laser-writing optical lithography,” *Adv. Mater.*, vol. 24, no. 20, pp. 2710–2714, 2012, doi: 10.1002/adma.201200584.

[20] S. Ahsan Khalid, A. M. Khan, and O. R. Shah, “Effects of the use of Auxectic Structures for structural damping in composite sandwich core panels for wind turbine blades,” *J. Energy Resour. Technol.*, pp. 1–23, 2020, doi: 10.1115/1.4048522.

[21] S. A. Khalid, A. M. Khan, and O. R. Shah, “A Numerical Study Into the Use of Auxectic Structures for Structural Damping in Composite Sandwich Core Panels for Wind Turbine Blades,” *J. Energy Resour. Technol.*, vol. 144, no. 3, 2022, doi: 10.1115/1.4051303.

[22] A. Sorrentino and D. Castagnetti, “Negative Poisson’s ratio lattice for designing vertebral biomaterials,” *Mech. Adv. Mater. Struct.*, vol. 29, no. 27, pp. 6626–6633, 2022, doi: 10.1080/15376494.2021.1983089.

[23] M. Kadic, T. Bückmann, N. Stenger, M. Thiel, and M. Wegener, “On the practicability of pentamode mechanical metamaterials,” *Appl. Phys. Lett.*, vol. 100, no. 19, 2012, doi: 10.1063/1.4709436.

[24] T. Bückmann, M. Thiel, M. Kadic, R. Schittny, and M. Wegener, “An elasto-mechanical unfeelability cloak made of pentamode metamaterials,” *Nat.*

Commun., vol. 5, 2014, doi: 10.1038/ncomms5130.

[25] T. Tancogne-Dejean, A. B. Spierings, and D. Mohr, "Additively-manufactured metallic micro-lattice materials for high specific energy absorption under static and dynamic loading," *Acta Mater.*, vol. 116, pp. 14–28, 2016, doi: 10.1016/j.actamat.2016.05.054.

[26] M. Hajhosseini and A. Mahdian Parrany, "A new periodic beam-like structure with special vibration-isolation characteristics," *Mech. Adv. Mater. Struct.*, vol. 29, no. 25, pp. 3804–3814, 2022, doi: 10.1080/15376494.2021.1910388.

[27] X. Wu, Y. Jin, A. Khelif, X. Zhuang, T. Rabczuk, and B. Djafari-Rouhani, "Topological surface wave metamaterials for robust vibration attenuation and energy harvesting," *Mech. Adv. Mater. Struct.*, vol. 29, no. 26, pp. 4759–4767, 2022, doi: 10.1080/15376494.2021.1937758.

[28] D. J. Sypeck and H. N. G. Wadley, "Cellular metal truss core sandwich structures," *Adv. Eng. Mater.*, vol. 4, no. 10, pp. 759–764, 2002, doi: 10.1002/1527-2648(20021014)4:10<759::AID-ADEM759>3.0.CO;2-A.

[29] G. W. Kooistra and H. N. G. Wadley, "Lattice truss structures from expanded metal sheet," *Mater. Des.*, vol. 28, no. 2, pp. 507–514, 2007, doi: 10.1016/j.matdes.2005.08.013.

[30] S. Chiras *et al.*, "The structural performance of near-optimized truss core panels," *Int. J. Solids Struct.*, vol. 39, no. 15, pp. 4093–4115, 2002, doi: 10.1016/S0020-7683(02)00241-X.

[31] B. Wang, J. Q. Hu, Y. Q. Li, Y. T. Yao, S. X. Wang, and L. Ma, "Mechanical properties and failure behavior of the sandwich structures with carbon fiber-reinforced X-type lattice truss core," *Compos. Struct.*, vol. 185, pp. 619–633, 2018, doi: 10.1016/j.compstruct.2017.11.066.

[32] U. G. K. Wegst, H. Bai, E. Saiz, A. P. Tomsia, and R. O. Ritchie, “Bioinspired structural materials,” *Nat. Mater.*, vol. 14, no. 1, pp. 23–36, 2015, doi: 10.1038/nmat4089.

[33] F. Tamburrino, S. Graziosi, and M. Bordegoni, “The design process of additively manufactured mesoscale lattice structures: A review,” *Journal of Computing and Information Science in Engineering*, vol. 18, no. 4. 2018. doi: 10.1115/1.4040131.

[34] A. du Plessis *et al.*, “Beautiful and Functional: A Review of Biomimetic Design in Additive Manufacturing,” *Additive Manufacturing*, vol. 27. pp. 408–427, 2019. doi: 10.1016/j.addma.2019.03.033.

[35] T. Maconachie *et al.*, “SLM lattice structures: Properties, performance, applications and challenges,” *Materials and Design*, vol. 183. 2019. doi: 10.1016/j.matdes.2019.108137.

[36] J. Fan *et al.*, “A review of additive manufacturing of metamaterials and developing trends,” *Materials Today*, vol. 50. pp. 303–328, 2021. doi: 10.1016/j.mattod.2021.04.019.

[37] A. Nazir and J. Y. Jeng, “Buckling behavior of additively manufactured cellular columns: Experimental and simulation validation,” *Mater. Des.*, vol. 186, 2020, doi: 10.1016/j.matdes.2019.108349.

[38] Z. Alomar and F. Concli, “A Review of the Selective Laser Melting Lattice Structures and Their Numerical Models,” *Advanced Engineering Materials*, vol. 22, no. 12. 2020. doi: 10.1002/adem.202000611.

[39] K. Refai, M. Montemurro, C. Brugger, and N. Saintier, “Determination of the effective elastic properties of titanium lattice structures,” *Mech. Adv. Mater. Struct.*, vol. 27, no. 23, pp. 1966–1982, 2020, doi:

10.1080/15376494.2018.1536816.

[40] L. J. Gibson and M. F. Ashby, “The mechanics cellular materials of three-dimensional cellular materials,” *Proc. R. Soc. L.*, vol. A382, pp. 43–59, 1982.

[41] V. S. Deshpande, N. A. Fleck, and M. F. Ashby, “Effective properties of the octet-truss lattice material,” *J. Mech. Phys. Solids*, vol. 49, no. 8, pp. 1747–1769, 2001, doi: 10.1016/S0022-5096(01)00010-2.

[42] V. S. Deshpande and N. A. Fleck, “Collapse of truss core sandwich beams in 3-point bending,” *Int. J. Solids Struct.*, vol. 38, no. 36–37, pp. 6275–6305, 2001, doi: 10.1016/S0020-7683(01)00103-2.

[43] R. G. Hutchinson and N. A. Fleck, “The structural performance of the periodic truss,” *J. Mech. Phys. Solids*, vol. 54, no. 4, pp. 756–782, 2006, doi: 10.1016/j.jmps.2005.10.008.

[44] V. S. Deshpande, M. F. Ashby, and N. A. Fleck, “Foam topology: Bending versus stretching dominated architectures,” *Acta Mater.*, vol. 49, no. 6, pp. 1035–1040, 2001, doi: 10.1016/S1359-6454(00)00379-7.

[45] M. Abdelhamid and A. Czekanski, “An experimental investigation of analytical vs. numerical lattice structure design tools,” *Mech. Adv. Mater. Struct.*, vol. 29, no. 25, pp. 3614–3622, 2022, doi: 10.1080/15376494.2021.1892887.

[46] B. Hanks, J. Berthel, M. Frecker, and T. W. Simpson, “Mechanical properties of additively manufactured metal lattice structures: Data review and design interface,” *Addit. Manuf.*, vol. 35, 2020, doi: 10.1016/j.addma.2020.101301.

[47] L. R. Meza *et al.*, “Reexamining the mechanical property space of three-dimensional lattice architectures,” *Acta Mater.*, vol. 140, pp. 424–432, 2017, doi: 10.1016/j.actamat.2017.08.052.

[48] L. J. Feng, L. Z. Wu, and G. C. Yu, “An Hourglass truss lattice structure and its mechanical performances,” *Mater. Des.*, vol. 99, pp. 581–591, 2016, doi: 10.1016/j.matdes.2016.03.100.

[49] P. Li, Z. Wang, N. Petrinic, and C. R. Siviour, “Deformation behaviour of stainless steel microlattice structures by selective laser melting,” *Mater. Sci. Eng. A*, vol. 614, pp. 116–121, 2014, doi: 10.1016/j.msea.2014.07.015.

[50] L. Liu, P. Kamm, F. García-Moreno, J. Banhart, and D. Pasini, “Elastic and failure response of imperfect three-dimensional metallic lattices: the role of geometric defects induced by Selective Laser Melting,” *J. Mech. Phys. Solids*, vol. 107, pp. 160–184, 2017, doi: 10.1016/j.jmps.2017.07.003.

[51] L. J. Feng, J. Xiong, L. H. Yang, G. C. Yu, W. Yang, and L. Z. Wu, “Shear and bending performance of new type enhanced lattice truss structures,” *Int. J. Mech. Sci.*, vol. 134, pp. 589–598, 2017, doi: 10.1016/j.ijmecsci.2017.10.045.

[52] L. Raimondi, L. Tomesani, L. Donati, and A. Zucchelli, “Lattice material infiltration for hybrid metal-composite joints: Manufacturing and static strenght,” *Compos. Struct.*, vol. 269, no. October 2020, p. 114069, 2021, doi: 10.1016/j.compstruct.2021.114069.

[53] G. Qi, B. Ji, and L. Ma, “Mechanical response of pyramidal lattice truss core sandwich structures by additive manufacturing,” *Mech. Adv. Mater. Struct.*, vol. 26, no. 15, pp. 1298–1306, 2019, doi: 10.1080/15376494.2018.1432805.

[54] M. N. Andersen, F. Wang, and O. Sigmund, “On the competition for ultimately stiff and strong architected materials,” *Mater. Des.*, vol. 198, 2021, doi: 10.1016/j.matdes.2020.109356.

[55] N. Triantafyllidis and W. C. Schnaidt, “Comparison of microscopic and macroscopic instabilities in a class of two-dimensional periodic composites,” *J.*

Mech. Phys. Solids, vol. 41, no. 9, pp. 1533–1565, 1993, doi: 10.1016/0022-5096(93)90039-I.

[56] S. P. Timoshenko, J. M. Gere, and W. Prager, "Theory of Elastic Stability, Second Edition," *J. Appl. Mech.*, vol. 29, no. 1, pp. 220–221, 1962, doi: 10.1115/1.3636481.

[57] G. Totaro, F. De Nicola, and P. Caramuta, "Local buckling modelling of anisogrid lattice structures with hexagonal cells: An experimental verification," *Compos. Struct.*, vol. 106, 2013, doi: 10.1016/j.compstruct.2013.07.031.

[58] J. Z. Gu and S. Cheng, "Shear effect on buckling of cellular columns subjected to axially compressed load," *Thin-Walled Struct.*, vol. 98, pp. 416–420, 2016, doi: 10.1016/j.tws.2015.10.019.

[59] Y. He, Y. Zhou, Z. Liu, and K. M. Liew, "Buckling and pattern transformation of modified periodic lattice structures," *Extrem. Mech. Lett.*, vol. 22, pp. 112–121, 2018, doi: 10.1016/j.eml.2018.05.011.

[60] A. Shitanaka, T. Aoki, and T. Yokozeki, "Comparison of buckling loads of hyperboloidal and cylindrical lattice structures," *Compos. Struct.*, vol. 207, pp. 877–888, 2019, doi: 10.1016/j.compstruct.2018.09.052.

[61] H. Tang, L. Li, and Y. Hu, "Buckling analysis of two-directionally porous beam," *Aerosp. Sci. Technol.*, vol. 78, pp. 471–479, 2018, doi: 10.1016/j.ast.2018.04.045.

[62] A. Vigliotti and D. Pasini, "Stiffness and strength of tridimensional periodic lattices," *Comput. Methods Appl. Mech. Eng.*, vol. 229–232, pp. 27–43, 2012, doi: 10.1016/j.cma.2012.03.018.

[63] M. S. Anderson, "Buckling of periodic lattice structures," *AIAA J.*, vol. 19, no. 6,

pp. 782–788, 1981, doi: 10.2514/3.51003.

[64] J.S.Przemieniecki, *Theory of matrix structural analysis*. Dover Publications Inc., 1968.

[65] Y. Wu and L. Yang, “The effect of unit cell size and topology on tensile failure behavior of 2D lattice structures,” *Int. J. Mech. Sci.*, vol. 170, 2020, doi: 10.1016/j.ijmecsci.2019.105342.

[66] J. H. Argyris, O. Hilpert, G. A. Malejannakis, and D. W. Scharpf, “On the geometrical stiffness of a beam in space-a consistent V.W. approach,” *Comput. Methods Appl. Mech. Eng.*, vol. 20, no. 1, pp. 105–131, 1979, doi: 10.1016/0045-7825(79)90061-6.

[67] Z. R. D. McGuire William, Gallagher Richard H., *Matrix Structural Analisys - 2nd Edition*, 2nd ed. Faculty Books, 200AD.

[68] R. J. Roark, W. C. Young, and R. Plunkett, “Formulas for Stress and Strain,” *J. Appl. Mech.*, vol. 43, no. 3, pp. 522–522, 1976, doi: 10.1115/1.3423917.

[69] R. R. Cook, D. S. Malkus, M. E. Pelsha, and R. J. Witt, “Concepts and Applications of Finite Element Analysis,” *John Wiley Sons Inc*, 2002.

List of Figures